Schweizerische Eidgenossenschaft
Confédération suisse
Confederazione Svizzera
Confederaziun svizra

Federal Department of the Environment, Transport, Energy and Communications DETEC

Swiss Federal Office of Energy SFOE
Energy Research and Cleantech Division

REEL Demo – Romande Energie ELectric network in local balance Demonstrator

Deliverable: 4a3 Operation of the battery storage systems for grid control, feeder dispatching

Demo site: Aigle

Developed by
Dr. Antonio Zecchino, Rahul Gupta and Prof. Dr. Mario Paolone EPFL DESL

[Lausanne, 25.03.2021]

1 Description of deliverable and goal

1.1 Executive summary

The core of this activity is to provide distribution system operators with tools for the optimal and grid-aware operation of utility-scale distributed battery energy storage systems (BESSs) in order to optimize the integration of stochastic distributed generation. The ultimate goal is the optimal control of active distribution networks with high penetration of stochastic (i.e., non-controllable) renewable-based generation. In particular, unscheduled fluctuations of the power exchanged with the upper grid level are minimised via the proposed control and scheduling framework, where we compute a dispatch plan in day-ahead using advanced forecasts of the aggregated prosumption and track it during the real-time operation using a grid-aware optimal power flow (OPF)-based control of the controllable BESS accounting for both grid constraints and BESS operational constraints. We experimentally validated the proposed control and scheduling strategy to dispatch the operation of a medium voltage active distribution network interfacing stochastic heterogeneous prosumers by using a grid-connected BESS as a controllable element coupled with a distributed monitoring infrastructure. In particular, the framework consists of two algorithmic layers. In the first one (day-ahead scheduling), an aggregated dispatch plan is determined, which is based on the day-ahead forecast of the prosumption and accounts for the operational constraints of grid and BESS state-of-energy. An adaptive data-driven scheme based on multi-variate Gaussian distribution is used to forecast the power consumption and photovoltaic generation and used as an input at the day-ahead stage. Then, the dispatch plan for the next 24 hours is computed using a scenario-based iterative AC OPF (Codistflow) algorithm, which accounts for forecasts of RESs and load profiles with 95% confidence interval with 1h time resolution. The second layer consists of real-time operation, where a grid-aware model predictive control determines the active and reactive power set-points of the BESS so that their aggregated contribution tracks the dispatch plan while obeying to BESS's operational constraints as well as the grid's ones. The grid constraints are modelled using the Augmented Relaxed OPF developed at the EPFL-DESL. The proposed control framework is validated by dispatching the operation of a 12kV/20MVA MV distribution network in Aigle, Switzerland (i.e. the REeL demonstrator) using a 1.5 MW/2.5 MWh BESS, which is controlled in real-time given the online grid state estimation enabled by the deployed distributed PMU-based sensing infrastructure.

1.2 Research question

The research question that this activity aims to respond is the following: how can distribution system operators and power suppliers operate utility-scale distributed BESSs with the aim of optimizing the integration of stochastic distributed generation while enforcing the physical grid constraints, namely the constraints on nodal

voltages, lines and transformer capacities?

1.3 Novelty of the proposed solutions compared to the state-of-art

The exploitation of controllable distributed generation (DG), flexible demand and storage systems is seen by the modern power system community as the most optimal approach for increasing the stochastic DG hosting capacity of active power distribution networks, while maintaining minimal the impact on the local grid infrastructure as well as the fluctuations of the power exchanged with the upper grid level.
In this regard, previous works have investigated and developed strategies for the day-ahead prediction of DGs' and loads' behavior, acting on the controllable BESS to compensate for predictions vs realizations mismatches taking place at the moment of the realization during real-time applications [1–3]. However, none of the works presented in the current literature implemented grid-aware OPF-based and validated such multi-layer optimal control framework in a utility MW-scale MV distribution grid, operated by a commercial distribution system operator (DSO).
Within this context, the core novelties of the proposed work are three-fold, and are identified as:

- Development of a scenario based day-ahead OPF-based dispatch process that considers the forecasts of loads and distributed generation.
- Development of a computationally-efficient intra-day OPF-based real-time control of the controllable resources to track the dispatch plan capable of leveraging the real-time knowledge of the system state made available by the PMUs.
- Validation of the proposed methodologies in a full-scale real environment via the REeL demonstrator site in Aigle, Switzerland.

1.4 Methodology description

The undertaken main activities are the following:

- Day-ahead dispatch plan computation.
- Real-time operation.
- Validation on an active MV grid by controlling a utility-scale BESS.

The proposed control framework consist of two phases, namely the *scheduling* and *real-time phase*. In the scheduling phase on the day before operations, a stochastic optimization problem computes an aggregated dispatch plan at the grid connection point (GCP), accounting for the uncertainties of demand and PV generation via scenarios, and constraints of the grid and battery energy storage with its model. In the real-time phase, a grid-aware model predictive control (MPC) computes the active

and reactive power set-points of the battery so that its contribution tracks the dispatch plan at the GCP while obeying to the constraints of the grid. The MPC problem leverages short-term forecasting of the demand and PV generation for better compensation of the incurred dispatch error.
For both the phases, we account for the constraints on the grid using convex optimal power flow models. For the day-ahead stage we use the so-called "Corrected DistFLow (CoDistFlow)" from [4] which is an iterative approximation of the non-linear power flow. In brief, CoDistFlow approximate the non-linear OPF using DistFlow model by ignoring the grid losses which are corrected by performing true non-linear power flow on the optimized variables post-optimization. This iterative process is followed till convergence.
For the real-time operation, we utilize Augmented Relaxed Optimal Power Flow (AR-OPF) which presents a much better approximation compared to the other convex models [5]. This model allows us to have exact convex modeling of the non-linear power flow equations as proved in [5].
We refer to two-port equivalent Π model of the transmission circuit of Fig. 1 to model the constraints of the grid branches.

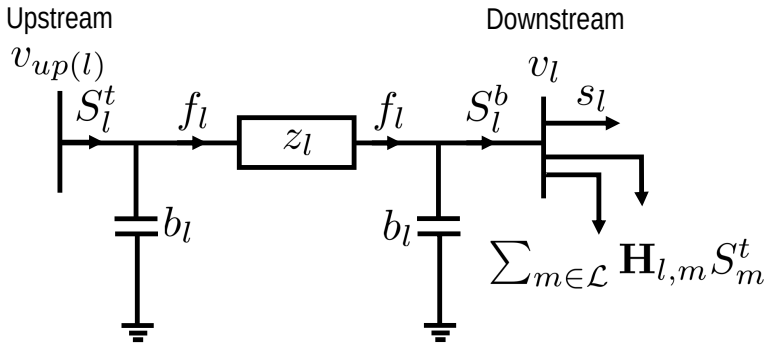

Figure 1: Illustration of the adopted nomenclature with respect to the classic two-port Π model of a transmission line.

In the following we present the day-ahead dispatch formulation and real-time model predictive control of the battery in detail.

Nomenclature

Co-dist flow variables (day-ahead)

$\epsilon_{t\phi}$ Uncovered dispatch error and time t, at scenario ϕSquare of current magnitude causing losses in line l at time t, scenario ϕ

$\psi_{lt\phi}$ Active power of the ESS at bus l that compensates for the dispatch error for time t and scenario phi

$\tilde{i}^b_{lt}$ Forecast current existing the line l at the bottom at time t

$\tilde{i}_{lt}$ Forecast current entering the line l from the top at time t

$\tilde{p}^L_{lt}$ Column vector of forecast active power correction terms for all lines, time t

$\tilde{q}^L_{lt}$ Column vector of forecast reactive power correction terms for all lines, time t

$\tilde{S}^t_{lt} = \tilde{P}^t_{lt} + j\tilde{Q}^t_{lt}$ Forecast of upstream complex power flow to line l at time t

$\tilde{s}_{lt} = \tilde{p}_{lt} + j\tilde{q}_{lt}$ Aggregated complex prosumption forecast at bus l at time t

$\tilde{v}^L_{lt}$ Column vector of forecast voltage square magnitude correction terms for lines l, time t

$\tilde{v}^S_{lt}$ Column vector of forecast voltage approximation for lines l, time t

$\tilde{v}_{lt}$ Square of voltage magnitude forecast at bus l at time t

F^B_{lt} Offset profile of the ESS at bus l at time t

$i^b_{lt\phi}$ Current existing the line l at the bottom at time t for scenario ϕ

$i_{lt\phi}$ Current entering the line l from the top at time t and for scenario ϕ

$p^L_{lt\phi}$ Column vector of active power correction terms for all lines, time t and scenario ϕ

$q^L_{lt\phi}$ Column vector of reactive power correction terms for all lines, time t and scenario ϕ

$S^t_{lt\phi} = P^t_{lt\phi} + jQ^t_{lt\phi}$ Upstream complex power flow to line l at time t at time ϕ

$s^B_{lt\phi} = p^B_{lt\phi} + jq^B_{lt\phi}$ Complex power flow of ESS at bus l at time t, scenario ϕ

$s_{lt\phi} = p_{lt\phi} + jq_{lt\phi}$ Aggregated prosumption at bus l at time t at scenario ϕ

$SoE_{lt\phi}$ Energy stored in ESS installed at bus l at time t at scenario ϕ

$v^L_{lt\phi}$ Column vector of voltage square magnitude correction terms for lines l, time t and scenario ϕ

$v^S_{lt\phi}$ Column vector of voltage approximation for lines l, time t and scenario ϕ

$v_{lt\phi}$ Square of voltage magnitude at bus l at time t, scenario ϕ

AR-OPF variables (real-time operation)

$\bar{f}_{lt}$ Auxiliary upper bound variable related to the square of current magnitude causing losses in line l at time t

$\bar{S}^b_{lt} = \bar{P}^b_{lt} + jQ^b_{lt}$ Auxiliary variable of complex power flow to bus l from line l at time t (upper bound of S^b_{lt})

$\bar{S}^t_{lt} = \bar{P}^t_{lt} + j\bar{Q}^t_{lt}$ Auxiliary variable of upstream complex power flow to line l at time t (upper bound of $S^t_l t$)

$\bar{v}_{lt}$ Auxiliary upper bound variable related to the square of voltage magnitude at bus l at time t

ϵ_t^* Uncovered dispatch error at time t

$\hat{S}_{lt}^b = \hat{P}_{lt}^b + j\hat{Q}_{lt}^b$ Auxiliary variable of complex power flow to bus l from line l at time t (lower bound of S_{lt}^b)

$\hat{S}_{lt}^t = \hat{P}_{lt}^t + j\hat{Q}_{lt}^t$ Auxiliary variable of upstream complex power flow to line l at time t (lower bound of S_{lt}^t)

ψ_{lt} Active power of the ESS at bus l that compensates for the dispatch error for time t

DP_t Dispatch plan associated with time t at the grid connecting point (GCP)

f_{lt} Square of current magnitude causing losses in line l at time t

$S_{lt}^b = P_{lt}^b + jQ_{lt}^b$ Downstream complex power flow to bus l from line l at time t

$S_{lt}^t = P_{lt}^t + jQ_{lt}^t$ Upstream complex power flow to line l at time t

$s_{lt}^B = p_{lt}^B + jq_{lt}^B$ Complex power flow of ESS at bus l at time t

$s_{lt} = p_{lt} + jq_{lt}$ Aggregated prosumption at bus l at time t

SoE_{lt} Energy stored in ESS installed at bus l at time t

v_{lt} Square of voltage magnitude at bus l at time t

Sets and Indices

$\phi \in \Phi$ Indices and set of scenarios

$f_{lt\phi}$

$l \in \mathcal{L}$ Indices and set of buses and indices of lines connected upstream to the buses

$t \in \mathcal{T}$ Indices and set of time intervals

$up(l)$ Indices of buses connected upstream to the line l

Parameters

$\alpha_l, \beta_l, \kappa_l$ Vectors defining the slope and the intercepts, respectively, of the set of lines which approximate the power capability curve of ESS at bus l

Δt Time duration of dispatch interval

Δ Weight coefficient to distribute the accumulated tracking error

γ_t Distributed energy correction at time t for the dispatch plan to compensate the accumulated tracking error

λ_ϕ Probability of scenario ϕ

$\mathbf{H}$ Adjacency matrix

b_l Half of the total shunt susceptance of line l

err Acculmated tracking error with respect to the dispatch plan

I_l^{max} Upper limit on the squared current of line l

N_c Allowed number of cycles per day chosen as a function of the targeted ESS lifetime

$P_l^{max} \backslash Q_l^{max}$ Upper limits of active\reacitve power flows for line l, respectively

SoE^{ini} Initial state-of-energy

SoE^{max} Maximum allowed state-of-energy level

SoE^{min} Minimum allowed state-of-energy level

T Time horizon of the daily OPF problem

$v^{max} \backslash v^{min}$ Upper bounds\Lower bounds of the squared nodal voltage magnitude

w_p, w_e, w_f Weight coefficient associated to the power flow at GCP, dispatch error, and the offset profile, respectively

$z_l = r_l + jx_l$ Total longitudinal impedance of line l

1.4.1 Day-ahead dispatch computation

The dispatch plan computation is performed by the operator in day-ahead before the real-time operation. The objective of the day-ahead scheduling is to compute the dispatch plan, mainly the active power trajectory that the targeted distribution network should follow at its grid connection point (GCP) during operations. The design requirements of the dispatch plan are:

- stochastic variations from the dispatch plan due to distributed generation and demand should be compensated by the controllable resources while respecting their operational constraints;
- the battery restore to certain State-of-Charge (SoC) for next-days operation.

The dispatch plan is computed with a stochastic optimization framework, where the stochastic injections of distributed generation and demand are modelled through forecast scenarios. Grid constraints are modelled using CoDistFlow. Operational constraints of the battery is modelled accounting for the PQ capability of their power converters and state-of-energy constraints. We model the battery losses by using a single-port electrical equivalent added as extra line in the existing grid as proposed in [4]. The main idea behind the proposed formulation is to determine a dispatch plan

that can be tracked for any of the forecast scenarios. The objective is to minimize the weighted sum of power at the GCP, distance among the scenarios and the dispatch plan and the offset profile of the battery.

$$\min_{\forall S^t, v, s^B, F^B} w_p \sum_{t\in\mathcal{T}} \sum_{\phi\in\Phi} \lambda_\phi P^t_{1t\phi} + w_e \sum_{t\in\mathcal{T}} \sum_{\phi\in\Phi} \lambda_\phi |\epsilon_{t\phi}| + w_f \sum_{t\in\mathcal{T}} \sum_{l\in\mathcal{L}} |F^B_{lt}|, \tag{1}$$

This problem is solved subject to the power balance constraints,

$$P^t_{lt\phi} = \sum_{k:\mathbf{H}_{lk}=1} P^t_{kt\phi} + p_{lt\phi} + p^B_{lt\phi} + p^L_{lt\phi}, \quad \forall l \in \mathcal{L}, \forall t \in \mathcal{T}, \forall \phi \in \Phi, \tag{2a}$$

$$Q^t_{lt\phi} = \sum_{k:\mathbf{H}_{lk}=1} Q^t_{kt\phi} + q_{lt\phi} + q^B_{lt\phi} - (v_{up(l)t\phi} + v_{lt\phi}) b_l/2 + q^L_{lt\phi}, \quad \forall l \in \mathcal{L}, \forall t \in \mathcal{T}, \forall \phi \in \Phi, \tag{2b}$$

voltage constraints,

$$v_{lt\phi} = v_{up(l)t\phi} - 2\Re\{z^*_l (S^t_{lt\phi} + j v_{up(l)t\phi} b_l/2)\} + v^L_{lt\phi}, \quad \forall l \in \mathcal{L}, \forall t \in \mathcal{T}, \forall \phi \in \Phi, \tag{3a}$$

$$v_{up(1)t\phi} = 1, \quad \forall l \in \mathcal{L}, \forall t \in \mathcal{T}, \forall \phi \in \Phi, \tag{3b}$$

$$v^2_{min} \leq v_{lt\phi} \leq v^2_{max}, \quad \forall l \in \mathcal{L}, \forall t \in \mathcal{T}, \forall \phi \in \Phi, \tag{3c}$$

current constraints,

$$\Re\{i_{lt\phi}\} = \frac{P^t_{lt\phi}}{v^S_{up(l)t\phi}}, \qquad \Im\{i_{lt\phi}\} = \frac{Q^t_{lt\phi}}{v^S_{up(l)t\phi}}, \quad \forall l \in \mathcal{L}, \forall t \in \mathcal{T}, \forall \phi \in \Phi, \tag{4a}$$

$$\Re\{i^b_{lt\phi}\} = (P^t_{lt\phi} - p^L_{lt\phi})/v^S_{lt\phi}, \quad \forall l \in \mathcal{L}, \forall t \in \mathcal{T}, \forall \phi \in \Phi, \tag{4b}$$

$$\Im\{i^b_{lt\phi}\} = \Im\{i_{lt\phi}\} + (v_{up(l)t\phi} + v_{lt\phi}) \frac{b_l}{2v^S_{lt\phi}} - \frac{q^L_{lt\phi}}{v^S_{lt\phi}}, \quad \forall l \in \mathcal{L}, \forall t \in \mathcal{T}, \forall \phi \in \Phi, \tag{4c}$$

$$\|i_{lt\phi}\| \leq I^{max}_l, \quad \|i^b_{lt\phi}\| \leq I^{max}_l, \quad \forall l \in \mathcal{L}, \forall t \in \mathcal{T}, \forall \phi \in \Phi, \tag{4d}$$

battery constraints

$$p^B_{lt\phi} = \psi_{lt\phi} + F^B_{lt}, \quad \forall l \in \mathcal{L}, \forall t \in \mathcal{T}, \forall \phi \in \Phi, \tag{5a}$$

$$\alpha_l p^B_{lt\phi} + \beta_l q^B_{lt\phi} \leqslant \kappa_l R_l, \quad \forall l \in \mathcal{L}, \forall t \in \mathcal{T}, \forall \phi \in \Phi, \tag{5b}$$

$$SoE_{l(t+1)\phi} = SoE_{lt\phi} + \Delta t p^B_{lt\phi}, \quad \forall l \in \mathcal{L}, \forall t \in \mathcal{T} \forall \phi \in \Phi, \tag{5c}$$

$$SoE^{min} C_l \leq SoE_{lt\phi} \leq SoE^{max} C_l, \quad \forall l \in \mathcal{L}, \forall t \in \mathcal{T}, \forall \phi \in \Phi, \tag{5d}$$

$$SoE_{l(1)\phi} = SoE^{ini} * C_l, \quad \forall l \in \mathcal{L}, \forall t \in \mathcal{T}, \tag{5e}$$

$$SoE_{l(1)\phi} - 0.1 C_l \leq SoE_{l(T+1)\phi} \leq SoE_{l(1)\phi} + 0.1 C_l, \quad \forall l \in \mathcal{L}, \forall t \in \mathcal{T}, \forall \phi \in \Phi, \tag{5f}$$

$$\frac{\Delta t}{2 * 1h} \left|\omega p^B_{lt\phi}\right| \leq N_c C_l, \quad \forall l \in \mathcal{L}, \forall t \in \mathcal{T}, \forall \phi \in \Phi. \tag{5g}$$

Note that the capability constraints of the converter is approximated by (5b).

1.4.2 Real-time operation

In the following, we describe the real-time control problem for tracking the day-ahead dispatch plan. Its objective is to determine the set-point for the controllable resources (battery in this specific case) to track the dispatch plan while respecting the grid and resources constraints. The grid constraints are modeled by the AR-OPF which is an exact convex approximation of the non-linear power flow as described [5]. The problem is formulated as model predictive control and its objective is to minimize the energy error incurred over a 5-min horizon length with control set points actuated at each 30 sec. The objective function is a multi-objective minimization of the weighted sum of grid losses and the dispatch energy error incurred at the GCP for the receding horizon interval. The problem is given as,

$$\min_{\forall S,v,s^B} w_l \sum_{t\in\mathcal{T}}\sum_{l\in\mathcal{L}} r_l f_{lt} + w_e \sum_{t\in\mathcal{T}} \epsilon_t^*, \quad \forall l \in \mathcal{L}, \forall t \in \mathcal{T}, \tag{6}$$

subject to power balance constraints

$$S_{lt}^t = s_{lt} + s_{lt}^B + \sum_{m\in\mathcal{L}} \mathbf{H}_{l,m} S_{lt}^t + z_l\, f_{lt} - j(v_{up(l)t} + v_{lt}) b_l, \tag{7a}$$

$$S_{lt}^b = s_{lt} + s_{lt}^B + \sum_{m\in\mathcal{L}} \mathbf{H}_{l,m} S_{lt}^t, \quad \forall l \in \mathcal{L}, \forall t \in \mathcal{T}, \tag{7b}$$

$$\bar{S}_{lt}^t = s_{lt} + s_{lt}^B + \sum_{m\in\mathcal{L}} \mathbf{H}_{l,m} \bar{S}_{lt}^t + z_l f_{lt} - j(v_{up(l)t} + v_{lt}) b_l, \quad \forall l \in \mathcal{L}, \forall t \in \mathcal{T}, \tag{7c}$$

$$\hat{S}_{lt}^t = s_{lt} + s_{lt}^B + \sum_{m\in\mathcal{L}} \mathbf{H}_{l,m} \hat{S}_{lt}^t - j(\bar{v}_{up(l)t} + \bar{v}_{lt}) b_l, \quad \forall l \in \mathcal{L}, \forall t \in \mathcal{T}, \tag{7d}$$

$$\hat{S}_{lt}^b = s_{lt} + s_{lt}^B + \sum_{m\in\mathcal{L}} \mathbf{H}_{l,m} \hat{S}_{lt}^t, \quad \forall l \in \mathcal{L}, \forall t \in \mathcal{T}, \tag{7e}$$

$$\bar{S}_{lt}^b = s_{lt} + s_{lt}^B + \sum_{m\in\mathcal{L}} \mathbf{H}_{l,m} \bar{S}_{lt}^t, \quad \forall l \in \mathcal{L}, \forall t \in \mathcal{T}, \tag{7f}$$

voltage constraints

$$v_{lt} = v_{up(l)t} - 2\Re\Big(z_l^* \Big(S_{lt}^t + j v_{up(l)t} b_l \Big) \Big) + |z_l|^2 f_{lt}, \quad \forall l \in \mathcal{L}, \forall t \in \mathcal{T}, \tag{8a}$$

$$\bar{v}_{lt} = \bar{v}_{up(l)t} - 2\Re\Big(z_l^* (\hat{S}_{lt}^t + j \bar{v}_{up(l)t} b_l) \Big), \quad \forall l \in \mathcal{L}, \forall t \in \mathcal{T}, \tag{8b}$$

$$v^{min} \le v_{lt}, \;\; \bar{v}_{lt} \le v^{max}, \quad \forall l \in \mathcal{L}, \forall t \in \mathcal{T}, \tag{8c}$$

current and power constraints

$$f_{lt} \geq \frac{|S^t_{lt} + j v_{up(l)t} b_l|^2}{v_{up(l)t}}, \quad \forall l \in \mathcal{L}, \quad \forall t \in \mathcal{T}, \tag{9a}$$

$$\bar{f}_{lt} v_{lt} \geq |\max\left\{|\hat{P}^b_{lt}|, |\bar{P}^b_{lt}|\right\}|^2 + |\max\left\{|\hat{Q}^b_{lt} - j\bar{v}_{lt} b_l|, |\bar{Q}^b_{lt} - j v_{lt} b_l|\right\}|^2, \quad \forall l \in \mathcal{L}, \forall t \in \mathcal{T}, \tag{9b}$$

$$\bar{f}_{lt} v_{up(l)t} \geq |\max\left\{|\hat{P}^t_{lt}|, |\bar{P}^t_{lt}|\right\}|^2 + |\max\left\{|\hat{Q}^t_{lt} + j\bar{v}_{up(l)t} b_l|, |\bar{Q}^t_{lt} + j v_{up(l)t} b_l|\right\}|^2, \quad \forall l \in \mathcal{L}, \forall t \in \mathcal{T}, \tag{9c}$$

$$I^{max}_{lt} v_{up(l)t} \geq |\max\left\{|\hat{P}^t_{lt}|, |\bar{P}^t_{lt}|\right\}|^2 + |\max\left\{|\hat{Q}^t_{lt}|, |\bar{Q}^t_{lt}|\right\}|^2, \quad \forall l \in \mathcal{L}, \forall t \in \mathcal{T}, \tag{9d}$$

$$I^{max}_{lt} v_{lt} \geq |\max\left\{|\hat{P}^b_{lt}|, |\bar{P}^b_{lt}|\right\}|^2 + |\max\left\{|\hat{Q}^b_{lt}|, |\bar{Q}^b_{lt}|\right\}|^2, \quad \forall l \in \mathcal{L}, \forall t \in \mathcal{T}, \tag{9e}$$

$$\bar{P}^t_{lt} \leq P^{max}_{lt}, \qquad \bar{Q}^t_{lt} \leq Q^{max}_{lt}, \quad \forall l \in \mathcal{L}, \forall t \in \mathcal{T}, \tag{9f}$$

dispatch error constraint

$$\gamma_t = \Delta * (1 - \Delta)^{t-1} * err, \quad \forall t \in \mathcal{T}, \tag{10a}$$

$$|(DP_t + \gamma_t) - P^t_{1t}| \leq \epsilon^*_t, \quad \forall t \in \mathcal{T}, \tag{10b}$$

battery constraints

$$p^B_{lt} = \psi_{lt} + F^B_{lt}, \quad \forall l \in \mathcal{L}, \forall t \in \mathcal{T}, \tag{11a}$$

$$\alpha_l p^B_{lt} + \beta_l q^B_{lt} \leqslant \kappa_l R_l, \quad \forall l \in \mathcal{L}, \forall t \in \mathcal{T}, \tag{11b}$$

$$SoE_{l(t+1)} = SoE_{lt} + \Delta t p^B_{lt}, \quad \forall l \in \mathcal{L}, \forall t \in \mathcal{T}, \tag{11c}$$

$$SoE^{min} C_l \leq SoE_{lt} \leq SoE^{max} C_l, \quad \forall l \in \mathcal{L}, \forall t \in \mathcal{T}, \tag{11d}$$

$$SoE_{l(1)} = SoE^{measured} * C_l, \quad \forall l \in \mathcal{L}, \forall t \in \mathcal{T}, \tag{11e}$$

$$\frac{\Delta t}{2 * 1h} \left|\omega p^B_{lt}\right| \leq N_c C_l, \quad \forall l \in \mathcal{L}, \forall t \in \mathcal{T}, \tag{11f}$$

1.5 Validation on an active MV grid by controlling a utility-scale BESS

1.5.1 Experimental Setup

The medium voltage (MV) distribution grid hosting the full-scale field validation is located in the municipality of Aigle, Vaud, Switzerland and is operated by the local distribution grid operator Romande-Energie. It has a nominal voltage of 21 kV. The MV grid is operated in radial configuration and consist of 24 nodes, the topology is shown in Fig 2. The MV grid hosts a high level of distributed renewable-based generation, namely 3.4 MVA of hydroelectric generation and 3.2 MWp of rooftop photovoltaics, including a 1.8 MWp single plant. As shown in the Fig 2, the considered MV grid hosts 17 phasor measurement units (PMUs) as shown in Fig 2 and 5 distributed along the feeder. Such PMU-based sensing infrastructure enables the continuous collection of grid measurements at 20 ms resolution, as well as the real-time estimation of the grid status also at nodes where no units are installed, which is considered as input for the real-time OPF-based BESS control. Furthermore, three Global Irradiance and Temperature (GIT) measurements boxes have been installed at

the large MW-scale PV plant show in Fig. 4 to provide environmental information at different points of the site. This information is used both for historical weather data analysis and for the real-time awareness of the PV plant conditions, also employed for short-term forecasting of its generation.

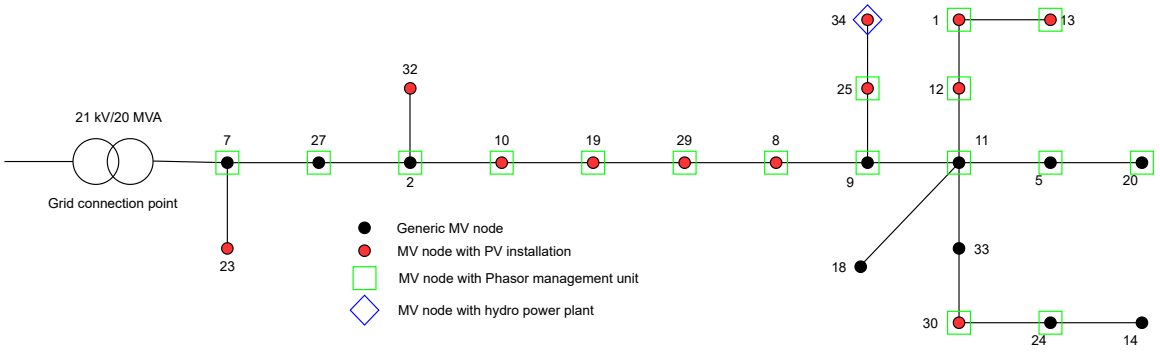

Figure 2: Grid layout of the considered 20 kV Medium Voltage (MV) distribution network at Aigle, Switzerland.

Figure 3: Battery installation: interior view of the battery container located at node 11 of the considered MV grid.

The technical specifications of the 1.5 MW/2.5 MWh BESS, including information of its cell technology as well as of its power conversion system (PCS) are included in Table 1.

1.5.2 Implementation of the algorithms

Figure 6 shows the sequence of operations and communication flow among of the day-ahead scheduler and real-time controller. In the former phase (upper dashed rectangle), the dispatch plan is computed and stored in the time series database. In the latter (lower dashed rectangle), a real-time local SCADA, the short-term forecasters, and controllable resources save their outputs in the same database (at 1 sec resolution). The real-time controllers access this information to compute the control actions, which are then sent to the controllable resources for actuation through

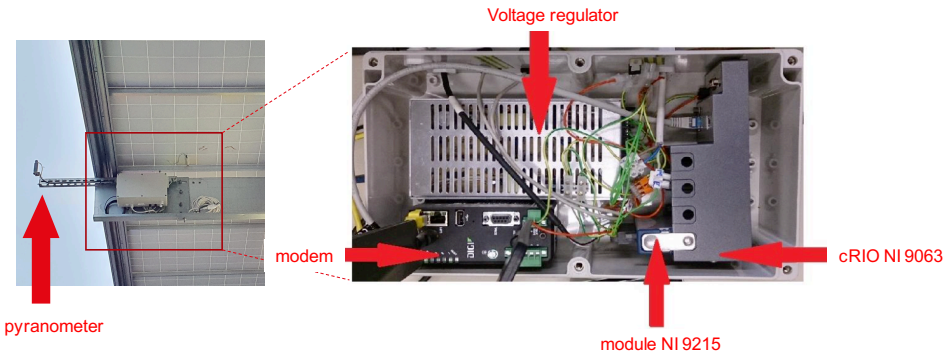

Figure 4: GHI and temperature measurement (GIT) box: (left) installation on site, (b) components: NI cRIO 9063 with module 9215, 4G modem and power source. This device is located at node 12.

Figure 5: Adopted PMU by Zaphiro Technologies with GPS antenna and current and voltage sensors (left) and installation at the Aigle demonstrator site (right).

UDP. The set-points are sent continuously to minimize packet losses.

1.5.3 Forecasting of the demand and PV generation

As described before, the day-ahead dispatch plan computation is a scenario-based optimization, thus it requires day-ahead scenarios of the demand and the distributed renewable generation. We use a Markov's chain based forecasting scheme to model the day-ahead demand scenarios which first cluster the demand into different day-types and estimate forecasting model for each of the cluster using multi-variate Gaussian distribution accounting for the correlation between the intra-day time steps. For the day-ahead PV scenarios, we correct GHI forecast of MeteoSwiss[1] using historical realization measured using our GITboxes installed at the experimental site.

Real-time demand and PV forecasting are based on persistent prediction; thanks to our invasive grid sensing infrastructure such as PMUs and pyranometers for GHI measurements, we have access to the latest values of nodal injections and GHI vari-

[1]https://www.meteoswiss.admin.ch

Table 1: Technical specifications of the 1.5 MW/2.5 MWh BESS installed at the 21 kV MV grid of Romande Energie in Aigle, Vaud, Switzerland.

Parameter	**Value**
Nominal capacity	1.5 MVA/2.5 MWh
GCP Voltage	21 kV
DC bus voltage range	770-1000 V
PCS PQ controllability	4-quadrant operation
PCS efficiency	93 % for all the operating conditions
Total harmonic distortion	< 3 %
CSC operation mode	Compliant
VSC operation mode	Compliant
Cell technology	Lithium nickel manganese cobalt oxide (NMC)
Number of racks	30 in parallel
Number of modules per rack	11 in series
Cells configuration per module	1p22s
Total number of cells	7260
Cell nominal voltage	3.68 (limits 2.7 - 4.15 V)
Cell nominal capacity	94 Ah (343 Wh)
Battery cycle life	4000 equivalent cycle at 1C rate at 100 % DoD with 80 % of the initial storage capacity available at the end of life

ation. We assume that this state will not be changed significantly in 5 sec.
More details on the forecasting method their validation is included in report "4d validation of an advanced control algorithms based on short-term forecasting of PV generation (RE Demo)" [6].

1.5.4 Experimental results

We present dispatch results for two distinct days. The first is a week-day and a cloudy day with high variation on the PV generation whereas the second is a weekend day with relatively clear-sky PV production.

9 March 2021 Figure 7 shows the results for day-ahead dispatch computation. Fig 7a shows the day-ahead aggregated scenarios at the GCP without the compensation of the battery. Fig. 7b shows the computed dispatch plan, scenarios at the slack with compensation of the battery and the battery offset profile designed to keep battery at optimum SOC level. As it can be observed all the scenario converge towards the dispatch plan with the help of the battery injections. Fig 9c shows the corresponding battery injections and SOC evolution for all the scenarios.
Figure 8 shows the results on real-time operation for the same day, it shows the power realization of the GCP with and without the compensation of the battery by MPC control in Fig. 8a. As it be observed, the dispatch plan is tracked over a 5-minute horizon with the help of the MPC control of the battery for almost whole day. The injection of the battery and SOC evolution is shown in Fig 8b. Fig 8c shows the cumulative distribution function (CDF) of the dispatch error with and without

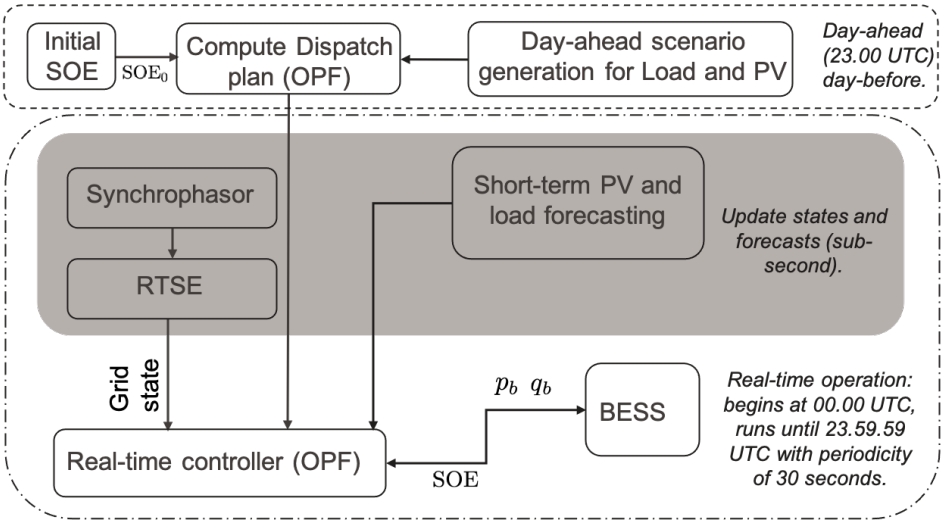

Figure 6: Implementation flow: Dispatch plan computation starts at 23.00 UTC day-before operation, using the PV and load forecasts, and is stored on the central data-server. Real-time operations start at 00.00 UTC. Synchrophasor and real-time state estimator (RTSE) and short-term forecasters store their outputs to the data server at sub-second scale, and real-time MPC controller computes power set-points for the buttery and actuates each 30 sec.

MPC using the compensation by the battery and computation time of the MPC. It can be observed that the dispatch error is mainly around 0 with MPC whereas it is spread over wide range of -500 kW to 1000 kW without MPC. The plot on the right shows that computation time is always within 10 sec which is 1/3rd of the control actuation time.

13 March 2021 Fig 9 shows the dispatch computation for a weekend day (Saturday) exhibiting different demand characteristic during the day. This day observed less PV production due to cloudy compared to the previous case. The predicted day-ahead scenarios are shown in Fig 9a and the corresponding computed dispatch plan is shown in Fig. 9b. We also show the scenarios at the GCP with battery compensation for the all the scenarios which tries to merge into the computed dispatch plan. The corresonding battery injections and SOC involution are shown in Fig. 9c. As it can be seen the battery is subjected to do its best to compensate the variation among the scenarios within its capability with respect to the constraint its capacity.
The real-time dispatch tracking using the OPF based grid-aware MPC is shown in Fig. 10. It shows the dispatch plan in black, the tracked power at the GCP in shaded gray and the power at the slack without MPC in red. As it can be observed that the MPC helps to track the dispatch plan during the day with its power compensation respecting the constraints of the grid and its own capacity. At one point when the battery is saturated, it stops charging, then after few time steps, it starts tracking again as the dispatch error results in discharging of the battery. The saturation of

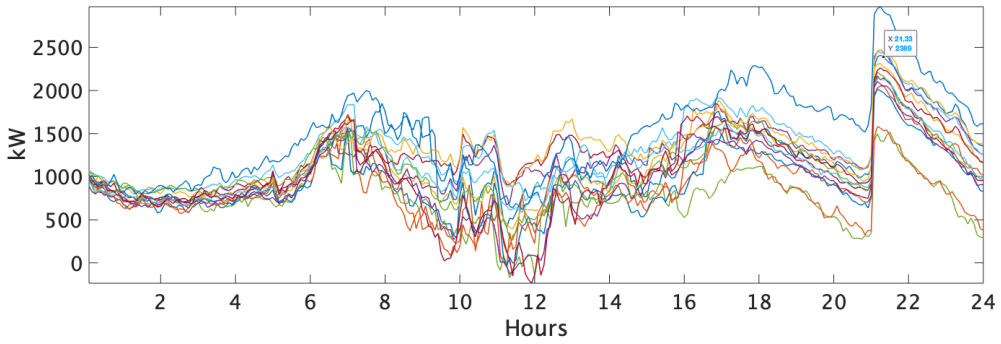

(a) Day-ahead aggregated prosumption scenarios at the GCP.

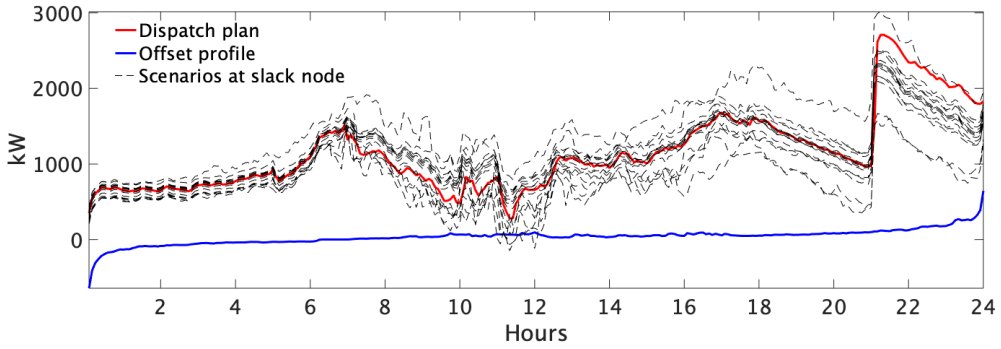

(b) Computed dispatch plan (in red), battery offset profile (in blue) and scenarios at GCP.

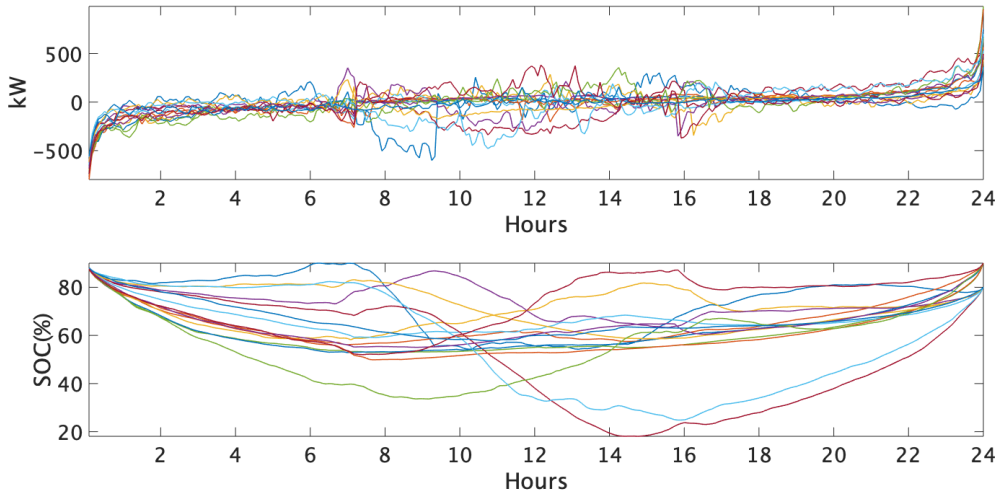

(c) Battery active power injection and SOC for different day-ahead scenarios.

Figure 7: (a-c) Dispatch plan computation for day 1 (9 March 2021).

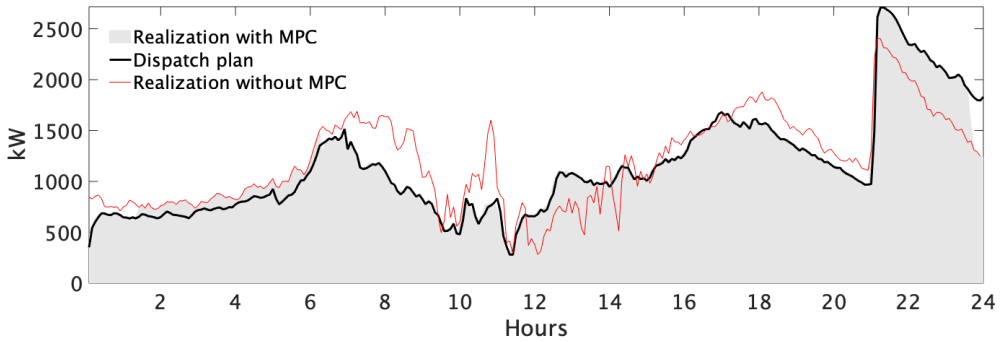

(a) Dispatch tracking: realized power at the GCP with and without MPC of the battery.

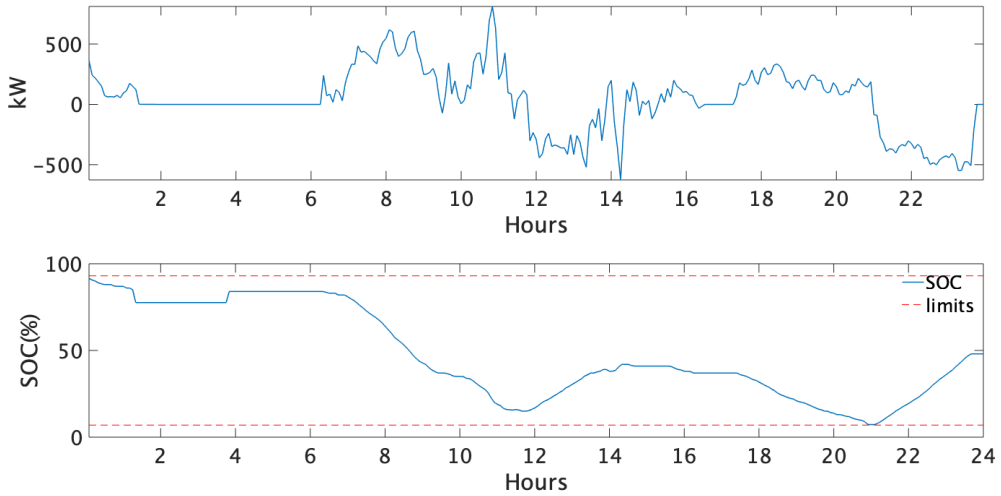

(b) Battery power compensation for tracking the dispatch plan (above), and corresponding SOC evolution (below).

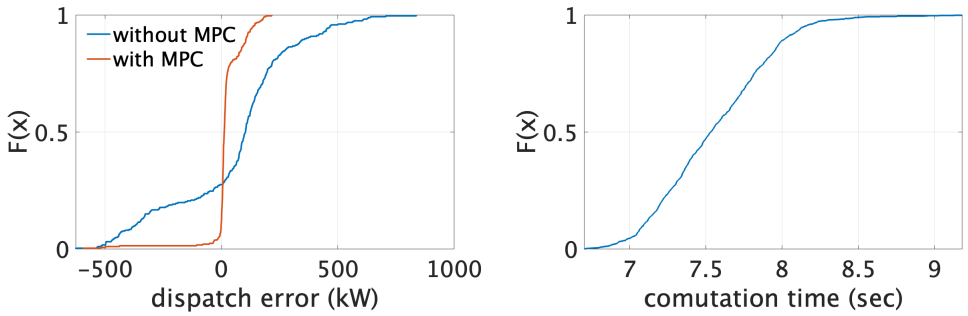

(c) Dispatch tracking performance with and without MPC (left) and time per MPC computation (right).

Figure 8: (a-b) Real-time tracking for day 1 (9 March 2021).

the battery might be due to imprecise prediction of the day-ahead scenarios and can be improved by more historical data into the forecasting tool. From the plot in Fig 8c, it can be observed that the dispatch error is mainly around 0 with MPC compared to the case without MPC. Also, the computation time is always below 10 sec suggesting that the MPC control actuation time can be further reduced than the current 30 sec.

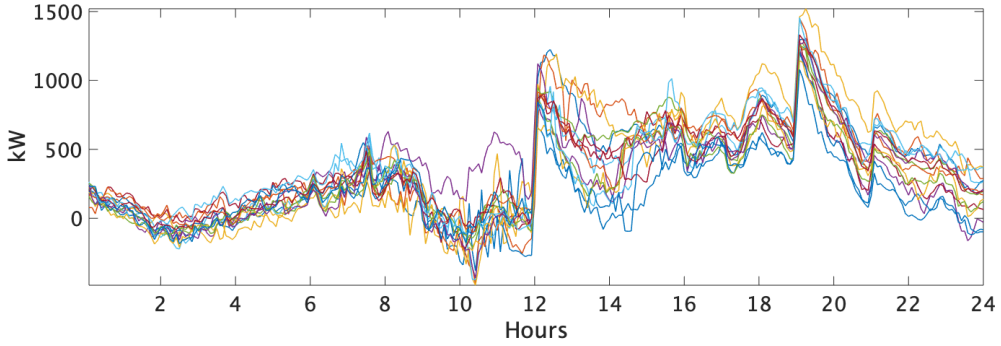

(a) Day-ahead aggregated prosumption scenarios at the GCP.

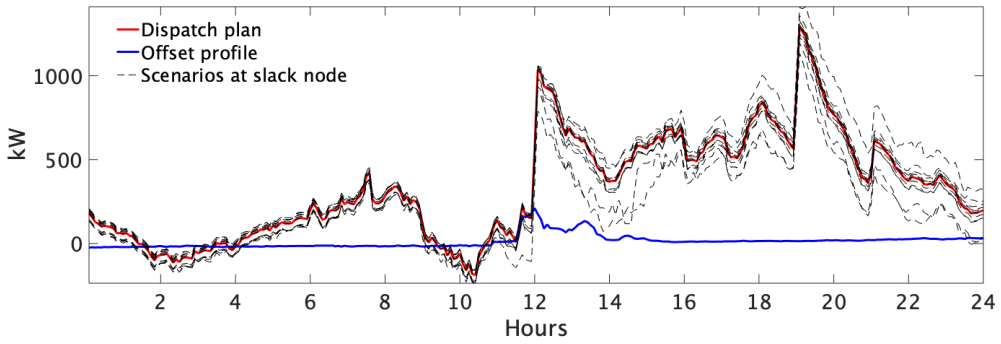

(b) Computed dispatch plan (in red), battery offset profile (in blue) and scenarios at GCP.

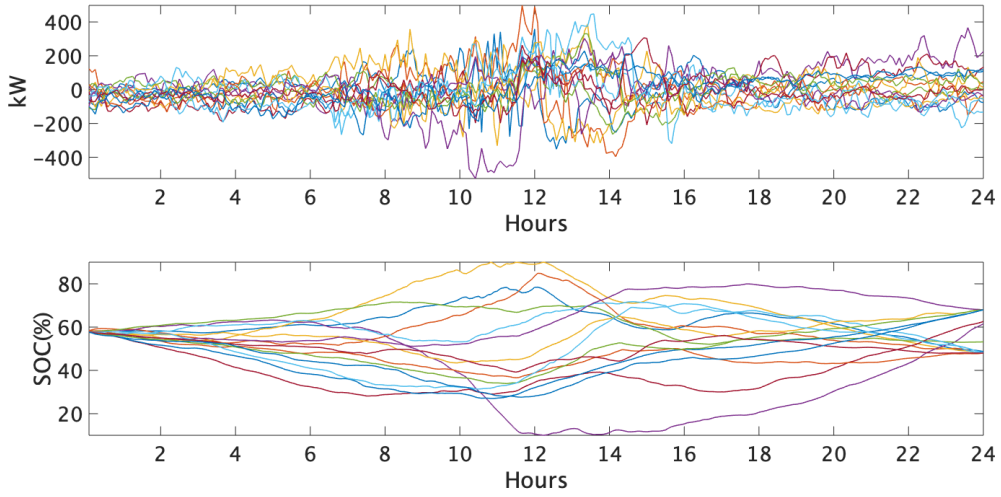

(c) Battery active power injection and SOC for different day-ahead scenarios.

Figure 9: (a-c) (a-c) Dispatch plan computation for day 2 (13 March 2021).

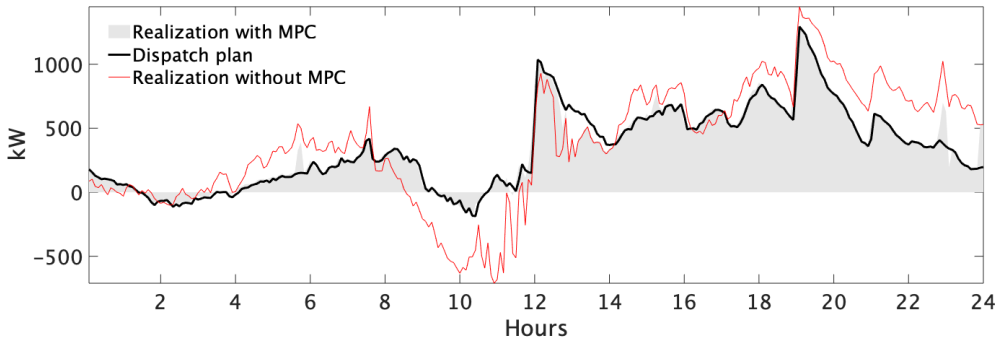

(a) Dispatch tracking: realized power at the GCP with and without MPC of the battery.

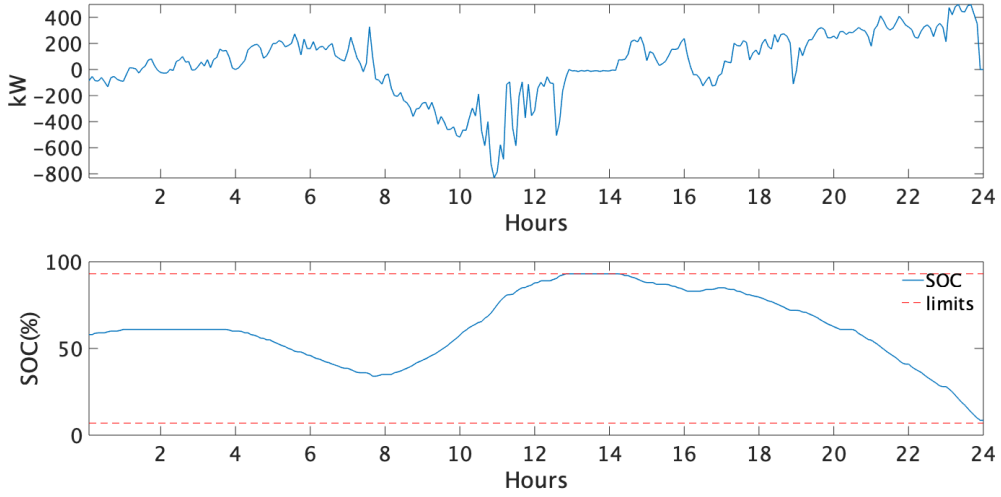

(b) Battery power compensation for tracking the dispatch plan (above), and corresponding SOC evolution (below).

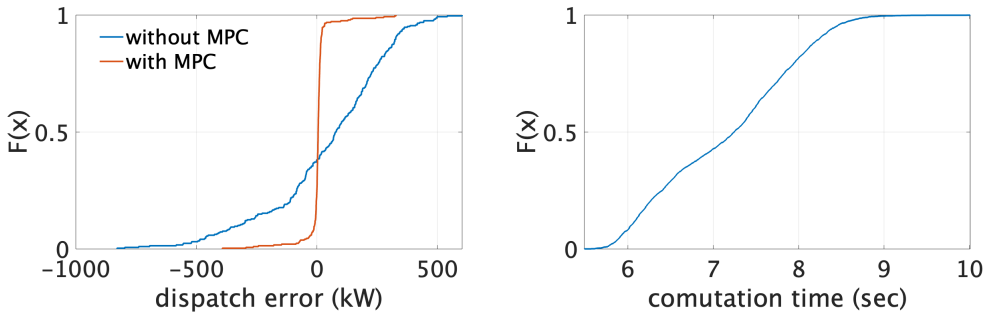

(c) Dispatch tracking performance with and without MPC (left) and time per MPC computation (right).

Figure 10: (a-b) Real-time tracking for day 2: 13 March 2021.

1.5.5 Validation of the grid constraints modeled by AR-OPF

We compare the voltage and current modeled by the real-time OPF with the PMU measurements on the site. The comparison is performed by plotting the CDF of the modeling error between the modelled quantities by the OPF and the measurements. We show error of the nodal voltage magnitudes, lines currents and grid losses. Figure 11 shows the cdfplot of the modelling error of the AR-OPF with respect true values (measured by PMUs). As it can be seen that maximum error on the voltage and current modelling are less than 0.01 pu and on the losses less than 0.2kW for 99 % of the time. This comparison validates that the OPF model used to model the grid constraints in real-time MPC are realistic.

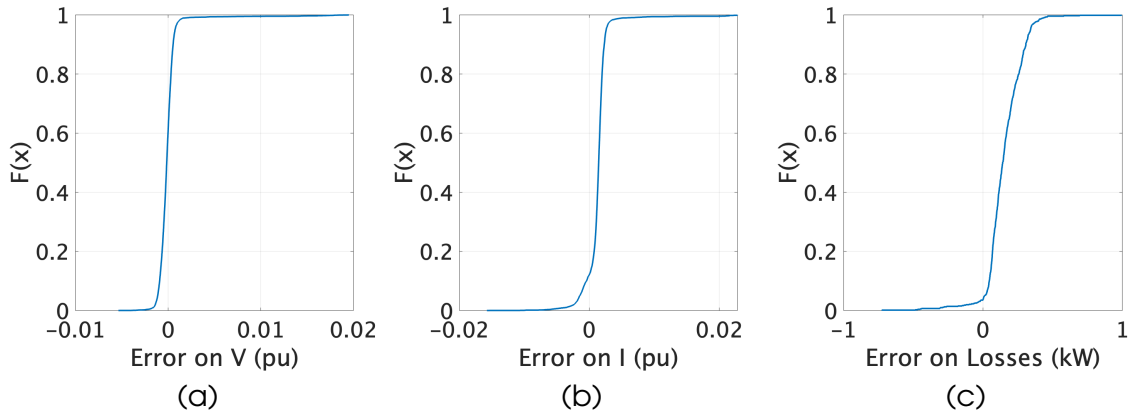

Figure 11: Validation of OPF model for real-time operation with PMU measurements: (a-c) shows cdfplot of the incurred error on the modeling of voltage (in pu), current (in pu) and total grid losses (in kW).

1.6 Regulatory and legal barriers for implementation

There is not any regulatory or legal barrier associated to the implementation of the proposed method per se. The only barriers encountered within the demonstration activities were on the accessibility of technical and operation data of the privately-owned distributed generation assets (small PVs and hydro power plants), which do not make their data publicly available in the first place.

2 Achievement of deliverable

2.1 Date

March 2021

2.2 Demonstration of the deliverable

This deliverable has been achieved through:

- the development of tools for scenario based day-ahead OPF-based dispatch process that considers the forecasts of loads and distributed generation;
- the development of a computationally-efficient intra-day OPF-based real-time control of the controllable resources to track the dispatch plan;
- leverage the PMU-based real-time state-estimation to define a grid-state aware OPF;
- the field validation of the proposed methodologies in a full-scale real environment via the REeL demonstrator site in Aigle.

3 Impact

This deliverables represent the final outcome of a series of activities undertaken in the frame of REeL project. This involves the development of the OPF-based con-trol methodology and PMU-based real-time grid state monitoring, both patented, as well as the demonstration of those solutions in the real-grid of Aigle. Further activities have also been incorporated such as the short-term fore-casting (4c), definition of operational limits of the feeder (4a1) and sizing and siting of a BESS (4a2).

References

[1] F. Sossan, E. Namor, R. Cherkaoui, and M. Paolone, "Achieving the dispatchability of distribution feeders through prosumers data driven forecasting and model predictive control of electrochemical storage," *IEEE Transactions on Sustainable Energy*, vol. 7, no. 4, pp. 1762–1777, Oct 2016.

[2] E. Namor, F. Sossan, R. Cherkaoui, and M. Paolone, "Control of battery storage systems for the simultaneous provision of multiple services," *IEEE Transactions on Smart Grid*, vol. 10, no. 3, pp. 2799–2808, 2019.

[3] R. K. Gupta, F. Sossan, and M. Paolone, "Grid-aware distributed model predictive control of heterogeneous resources in a distribution network: Theory and experimental validation," *IEEE Transactions on Energy Conversion*, pp. 1–1, 2020.

[4] E. Stai, L. Reyes-Chamorro, F. Sossan, J.-Y. Le Boudec, and M. Paolone, "Dispatching stochastic heterogeneous resources accounting for grid and battery losses," *IEEE Transactions on Smart Grid*, vol. 9, no. 6, pp. 6522–6539, 2017.

[5] M. Nick, R. Cherkaoui, J.-Y. Le Boudec, and M. Paolone, "An exact convex formulation of the optimal power flow in radial distribution networks including transverse components," *IEEE Transactions on Automatic Control*, vol. 63, no. 3, pp. 682–697, 2017.

[6] R. K. Gupta and M. Paolone, "Chapter on validation of an advanced control algorithms based on short-term forecasting of pv generation (RE Demo)," 2021.